From Design to Orbit: Engineering Sub-arcsecond CubeSat Pointing Performance on Pathfinder-3

Paaras S. Agrawal, Christian O. Fuller, Kyle R. Kung, Jeremiah J. DiMatteo
Terran Orbital Corporation
6800 Broken Sound Parkway NW, Boca Raton, FL 33487

ABSTRACT

Pathfinder-3 (PTD-3) spacecraft is the third vehicle of the NASA Pathfinder Technology Demonstrator (PTD) series, which are a collection of 6U CubeSats launched in Low Earth Orbit (LEO) to demonstrate innovative payload capabilities. The payloads are hosted on commercially developed satellites designed and manufactured by Terran Orbital Corporation (TOC) with a goal to support a wide array of technology demonstration missions through a flexible architecture that can be tailored for custom needs. PTD-3 hosts a high data rate laser communications payload that does not include its own pointing acquisition and control system, and, therefore, is dependent on accurate bus pointing to establish and maintain the space-to-ground (S2G) link for optical communication transmission.

Traditional CubeSat attitude control sensors (i.e. star trackers, gyros) are too coarse to achieve the pointing accuracy and bias requirements of less than 6.2 arcsec (30 μrad) and 3.1 arcsec (15 μrad), respectively. Thus, direct measurements of line-of-sight error from the laser communication payload is provided as feedback into the bus attitude control loop to achieve the pointing accuracy required for the mission. Standard bus attitude control without payload feedback, using star trackers, gyros, and reaction wheels, is implemented to achieve initial acquisition of the ground optical terminal. After acquisition, payload line-of-sight error measurements serve as the source of attitude control feedback for the bus to achieve finer pointing accuracy.

This paper presents the design of the spacecraft with a focus on the pointing control architecture, design drivers, preliminary performance predications, and performance evaluation of the on-orbit system. Key design and analysis topics impacting pointing performance centralized around payload-to-bus frame misalignments (both thermal and mechanical), high frequency-induced reaction wheel jitter in the presence of spacecraft flexible modes and mitigation strategies, reaction wheel zero crossings, and the role of TLE induced ephemeris propagation error. The discussion concludes with demonstrations of on-orbit pointing accuracy achieving approximately 0.75 arcsec (4.0 μrad) when payload feedback is in the loop. To the authors' knowledge, this is among the best CubeSat demonstrated bus pointing achieved while ground tracking. The sub-arcsecond accuracy is accomplished via a low-cost CubeSat architecture (no multi-stage pointing loops with gimbals, fine steering mirrors, etc.) that can be immediately applied to support other similar laser communication systems or observation payloads capable of providing the spacecraft with low noise small angle attitude error measurements.

INTRODUCTION

Pathfinder-3 (PTD-3) is the third spacecraft of the NASA Pathfinder Technology Demonstrator (PTD) series, which are a collection of 6U CubeSats with the goal to demonstrate innovative payload capabilities in Low Earth Orbit (LEO). Terran Orbital Corporation (TOC) designed and manufactured the CubeSat and integrated a laser communication payload provided by MIT Lincoln Laboratory (MIT LL) known as the Terabyte Infrared Delivery (TBIRD) system.

Table 1: Orbital Elements at Launch [05-25-22]

Parameter	Value
Orbit Type	Sun-synchronous
Apogee, Perigee	531km, 525km
Inclination	97.5°
Longitude of the ascending node	83.9°

PTD-3 was launched into a Sun Synchronous Orbit (SSO) on a SpaceX Transporter-5 mission on May 25, 2022. The orbital elements immediately following deployment from the launch vehicle are shown in Table 1. The nominal operational period planned for PTD-3 was 4-months, however given the on-going successful mission demonstrations, operations were extended and have now continued for over 2 years.

PTD-3's primary mission is to demonstrate space-to-ground (S2G) laser communications via the TBIRD payload, which enables data transfer rates well beyond those capable by traditional RF communications.[1] PTD-3 has primarily been executing operations with the Optical Communications Telescope Laboratory (OCTL) in Mountain, CA.

Table 2: Vehicle Pointing Comparison for CubeSat Class Missions[2,3,4,5,6,7,8]. A standard control stage refers to a closed-loop control loop comprising of RWA, IMUs, and STs

Vehicle	Deployment Date	Pointing Accuracy	Control Stage	Mass [kg]
ASTERIA	20-Nov-17	0.5 arcsec RMS over 20m 2.6 arcsec RMS over 20m	2-stage control with piezo Standard with Payload Feedback	10.165
MinXSS-1	16-May-16	15-42 arcsec (3σ)	Standard	3.52
OCSD AC-7B&C	06-Dec-17	86.4 arcsec (3σ)	Standard	2.3
PTD-3	**25-May-22**	**0.75 arcsec RMS**	**Standard with Payload Feedback**	**11.38**
Argomoon+	16-Nov-22	36 arcsec	Standard	14
EQUULEUS+	16-Nov-22	288 arcsec (3σ)	Standard	11.5
HARP+	02-Nov-19	18000 arcsec RMS	Standard	6
PicSat++	22-Jan-12	30 arcsec RMS 1 arcsec RMS	Standard 2-stage control with piezo	3.5

+ requirement or design values

++ loss of mission

The payload does not have an independent pointing acqusition and control system, thus is reliant on bus steering to aquire and maintian a persistent S2G narrowband optical link with the OCTL. For a succesful mission, the PTD-3 spacecraft pointing accuracy and bias were required to be less than 6.2 arcsec (30 µrad) and 3.1 arcsec (15 µrad), respectively. Traditional CubeSat attitude control sensors do not meet the pefromance capabilities needed to meet the strict pointing accuracy needed for the mission. Thus, a novel pointing solution incorporating low noise, line-of-sight error measurments from the TBIRD payload as feedback into the bus attitude control loop was implemented. On-orbit performance of the bus has demonstrated 0.75 arcsec pointing accuracy on the worst-axis which is the best CubeSat bus pointing demonstrated at ground track rates to the authors' knowledge. A non-exhasutive comparison of pointing capabilities among similar class vehicles is shown in Table 2.

This paper presents the design of the spacecraft with a focus on the pointing control architecture, design drivers, performance predictions via simulation and analysis, and performance evaluation of the on-orbit experiments.

SPACECRAFT OVERVIEW

Table 3: PTD-3 Mass Properties

Parameter	Value	Units
Mass	11.381	kg
Moment of Inertia	[0.50, 0.18, 0.47]	kg-m^2

The 6U CubeSat was designed to support a 5 kg payload in approximately 3U volume. Table 3 summarizes mass properties of PTD-3 and the vehicle architecture is visualized in Figure 1. The EPS consists of two tri-fold deployable solar arrays connected through a Maximum Power Point Tracking (MPPT) module to 12V batteries with 120 Wh of total storage. The spacecraft is capable of uplink and downlink over both S-band and UHF. The ADCS sensor suite consists of two star trackers, two coarse sun sensors, one inertial measurement unit (IMU), and one GPS and antenna. The actuators consist of three nano reaction wheels (NRWs) and three torque rods. A solar array drive assembly (SADA) was used to rotate the tri-fold solar arrays to a fixed orientation after bus and payload commissioning was completed. The SADA configuration during initial commissioning and the rotated nominal operations configuration of the vehicle can be seen in Figure 2. This was done to maximize solar power generation in the LVLH/NADIR attitude which is the primary vehicle pointing orientation outside of dedicated payload operations. The payload boresight points along the spacecraft +X axis, so the 90° SADA

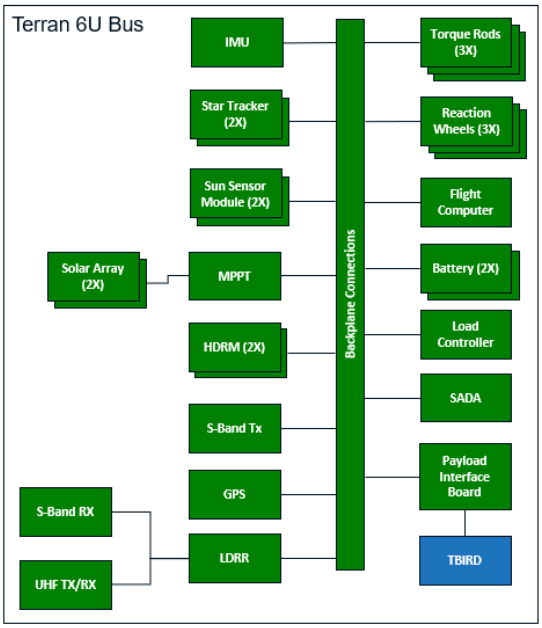

Figure 1: Spacecraft Architecture

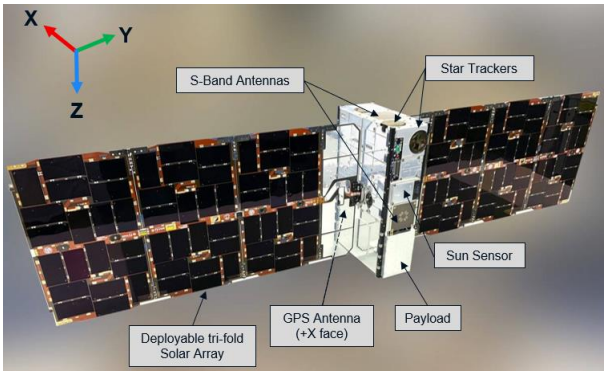

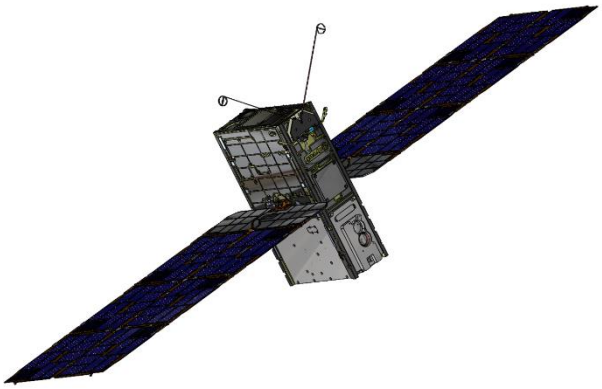

Figure 2: SADA configuration at launch (top) and SADA rotated 90° for nominal operations (bottom)

rotation also shifts the 1st flexible mode (i.e. floppy axis) from the solar array into the payload boresight roll axis. This mostly decouples the solar array 1st mode from the

cross-boresight direction and enables implementation of higher closed loop control bandwidths in the axes with strict pointing requirements.

GNC DEVELOPMENT AND DESIGN DRIVERS

The GNC implementation leveraged a suite of legacy flight validated algorithms alongside custom software developed to satisfy the mission specific requirements for the PTD-3 mission. The design and incorporation of payload feedback into the pointing architecture drove much of the custom GNC software development. This mission specific software was readily integrated into the existing flight legacy software given the philosophy of modularity followed by and engrained in the GNC software architecture. This principal of modularity enables rapid prototyping for algorithm testing within a flight code repository that has an extensive heritage of accumulated flight hours.

Key analysis and design topics centralized on closed loop controller design, initial acquisition in the presence of large bus-to-payload misalignments, quantifying reaction wheel jitter, impact on pointing performance in

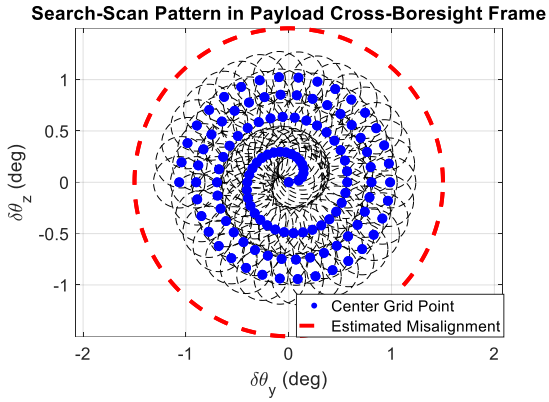

Figure 3: Scan pattern scans a region that is larger than the payload FOV.

the presence of flexible modes, bounding the quantity and impact of reaction wheel zero crossings over the mission, TLE propagation errors, and high fidelity closed-loop bus simulation performance. Assimilated pointing budgets aggregated the individual error sources into a final predicted capability which was used for design verification against the key pointing requirements. These topics will be discussed in the following sections.

Initial Acquisition

Acquisition pointing (pointing without the payload in the loop) utilizes ST and gyro measurements blended in a stellar inertial attitude determination (SIAD) algorithm alongside a control architecture leveraging reaction wheels used for steering and torque rods for momentum management.

On-board navigation algorithms produce state estimates of the vehicle's position, velocity, and attitude. These state estimates are used to generate attitude guidance reference commands, which are configurable to support various spacecraft tasking and operational modes (downlinking, lasercomm operation, low drag pointing, sun pointing). Attitude control errors are generated from the difference between the reference attitude and the estimated attitude. This control error is passed through a PID control loop whose output is body torque commands. These commands are translated to reaction wheel torques or speed commands based on reaction wheel mapping matrices.

The payload has a 0.25° FOV which drove an equivalent acquisition pointing requirement. Mounting misalignment between the payload boresight and spacecraft attitude determination frame typically exceed the payload FOV and are predicted on the order of 1-2°. As a result, there was significant risk in the ability to attain payload initial acquisition. To mitigate the misalignment error, an algorithm was implemented to

dynamically search through a preconfigured spiral pattern until acquiring valid signal data from the payload. The boresight is designed to dwell for a short, configured period on a grid point to allow for signal acquisition before proceeding through to the next grid location. Through a dynamic sweep, the estimated boresight would traverse through an effective FOV that is much larger than the 0.25° to increase probability of signal acquisition. The spiral pattern can be visualized in Figure 3 and shows how the boresight traverses an area sufficiently large enough to cover the predicted 1-2° misalignment. Note the radius of the spiral pattern can easily be increased through software configuration to scan a larger FOV in case of larger misalignments.

After signal acquisition is achieved (indicating a success in establishing the S2G link), the GNC software transitions to closed loop control utilizing line-of-sight measurements from the payload as feedback into the bus attitude controller. Note that after the first successful acquisition, the misalignment can be calibrated through telemetry analysis, and subsequent passes can use this knowledge to generate an attitude reference command that leads to a near guarantee of signal acquisition without the need for further execution of the search algorithm. Additional payload boresight shifts after initial acquisition is predicted to be much less than the 0.25° FOV. The option to enable or disable the search algorithm can be configured readily through a few simple configuration commands to the spacecraft.

To further mitigate the risk of payload misalignment errors preventing initial acquisition, a ground calibration measurement was performed on the fully assembled spacecraft prior to delivery to the launch vehicle. The pre-launch misalignment was measured to be 1.2°. This misalignment error was accounted for in the spacecraft attitude reference command to align the payload boresight prior to attempting lasercomm acquisition passes on-orbit. An additional 0.2° shift was observed between the pre-launch estimate and the recalibrated on-orbit estimate caused by vibrations that occurred during launch and deployment. Given the 0.2° shift was within the payload FOV of 0.25°, a valid payload link was detected on the first lasercomm pass attempt during initial acquisition, so the search algorithm was not needed.

Payload-in-the-loop Pointing Control

The payload utilizes a quad cell to detect the uplink beacon signal to provide a line-of-sight error measurement to the receive aperture onboard the payload.[1] This measurement is incorporated as feedback into the bus attitude controller and is the performance metric defining bus pointing accuracy.

Once the payload acquires signal with the optical ground terminal, the attitude control loop transitions to finer pointing via the incorporation of the line-of-sight error measurements provided by the payload. This payload in the loop control architecture is shown in Figure 4. An additional point-ahead term is added to the control error to account for the relative motion of the vehicle to the ground target and the finite speed of light.

Attitude control is achieved through a similar PID scheme to the nominal architecture, however instead of an augmented rate loop for all axes, the Y and Z axes use derivative control on the payload line-of-sight error signal, while the X axis continues to utilize gyro feedback. The gains for this controller are tuned to achieve a higher closed loop bandwidth to satisfy the pointing requirements.

Jitter Study

Quantifying spacecraft pointing errors induced by high frequency disturbances (such as NRWs) is critical to spacecraft line-of-sight performance on systems with strict pointing requirements. A jitter analysis was conducted to understand the effect of NRW induced disturbances on payload pointing. The PTD-3 NRWs are developed and manufactured internally by TOC with the performance needs of the CubeSat at the core of the design and manufacturing process. Each wheel is

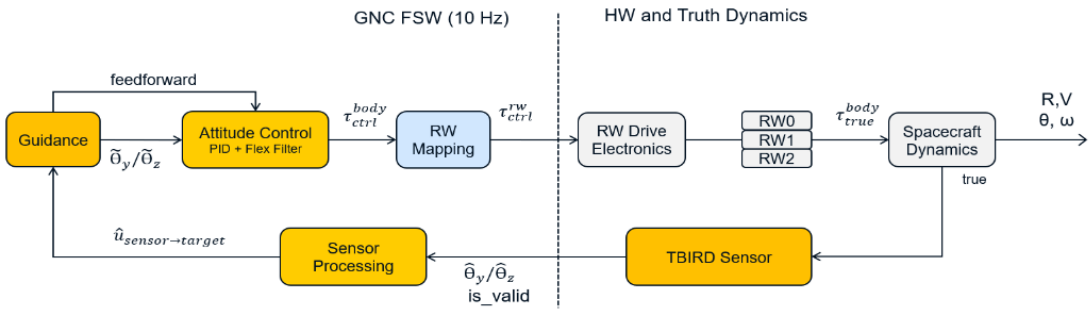

Figure 4: Payload-In-The-Loop Control Block Diagram

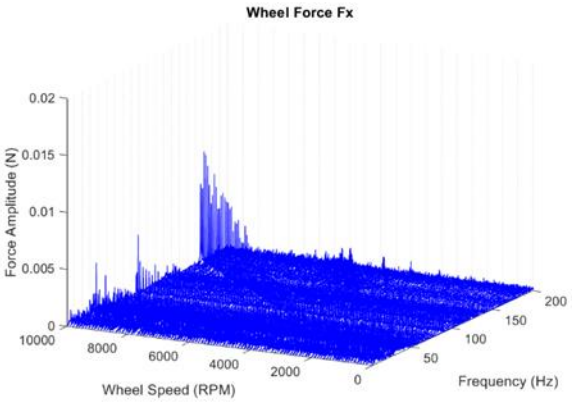

Figure 5: Measured NRW F_x Disturbance

capable of 6 mNm torque output and 50 mNms momentum storage with a maximum wheel speed of 10,000 RPM. The wheel can be operated in either a torque or speed control mode. For PTD-3 the speed mode operation was baselined. As part of the manufacturing process, each NRW is laser balanced to minimize force and torque disturbances on the spacecraft. Additionally, as part of acceptance testing, each wheel is strapped to a Kistler table where 3-axis force and 3-axis torque disturbances are measured at each wheel speed. Figure 5 shows the F_x disturbance for one of the NRW flight units. For typical NRWs, static imbalance values are on the order of 0.1 to 0.2 g-mm, with dynamic imbalance ranging from 10 to 15 g-mm^2. Imbalance terms are useful metrics to understanding the relative disturbance magnitudes of the first harmonic induced by different reaction wheel manufacturers. While this can be useful to compare wheel performance to first order, higher harmonics (2nd, 3rd, etc.) along with the location of wheel structural modes can drive significant force and torque disturbances that may affect spacecraft pointing stability. Given TOC wheel disturbance profiles are fully

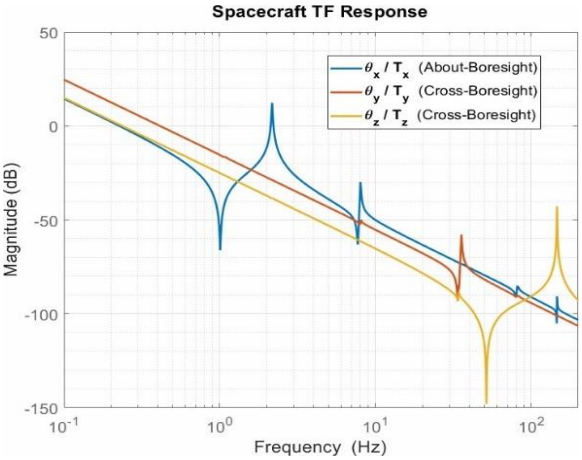

Figure 6: Spacecraft FEM. Pointing angle response to reaction wheel torques.

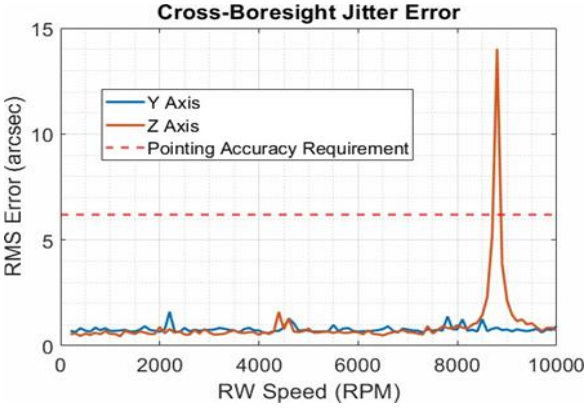

Figure 7: Jitter induced by reaction wheel disturbance when all wheels are operating at the same speed

characterized during Kistler testing, the full resolution frequency disturbance test data could be integrated into a jitter analysis.

The Power Spectral Density (PSD) disturbance profiles of the flight NRW units were injected into a Finite Element Model (FEM) of the bus to understand and analyze the pointing error induced by the RWA. The FEM included 26 spacecraft modes in a state-space model but did not include a fully integrated payload model. The transfer function response of the SC can be seen in Figure 6.

Given the desire to mitigate cross-boresight jitter the vehicle's solar arrays were rotated from 0° to 90°. This was achieved through use of a SADA onboard the vehicle and can be seen in Figure 2. About boresight (roll-axis) jitter does not appreciably degrade payload performance.

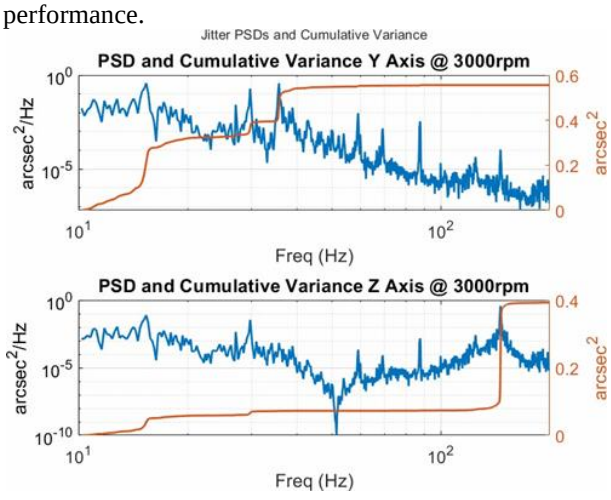

Figure 8: Output PSDs and cumulative variance for wheel speeds at 3000 RPM

As a result, the key spacecraft solar array resonance, at ~1Hz, is coupled with the payload about-boresight axis

and hence cross-boresight jitter is minimized. The per-axis RMS error is shown in Figure 7. The analysis shown assumes all three wheels are operating at the same wheel speed. While not practical in operation, this analysis assumption provides valuable insight into pointing sensitivity across the wheel speed spectrum. The output PSDs and a cumulative variance are shown in Figure 8 for all wheel speeds operating at 3000 RPM. Large increase in the cumulative variance indicates frequency regimes where corresponding large disturbances of pointing error occur. In nearly all wheel speed cases, the RMS error for both axes is less than 1 arcsec. A noticeable deviation occurs at 9000 RPM where the first harmonic of the RWA at 148Hz couples into the structural mode affecting primarily Z-axis pointing. This structural mode is clearly indicated in the spacecraft FEM shown in Figure 6 also at 148Hz. Given the reaction wheel speed range will nearly always be less than 3000 RPM the RWA induced jitter disturbance was not a large enough source of pointing error prevent meeting the bus pointing accuracy requirements.

Reaction Wheel Zero Crossings

The effect of reaction wheel zero crossings on pointing error was of central focus throughout the design and analysis process. Stiction occurring near zero crossings was suspected to cause undesirable pointing disturbance. Exaggerated stiction models, derived from flight

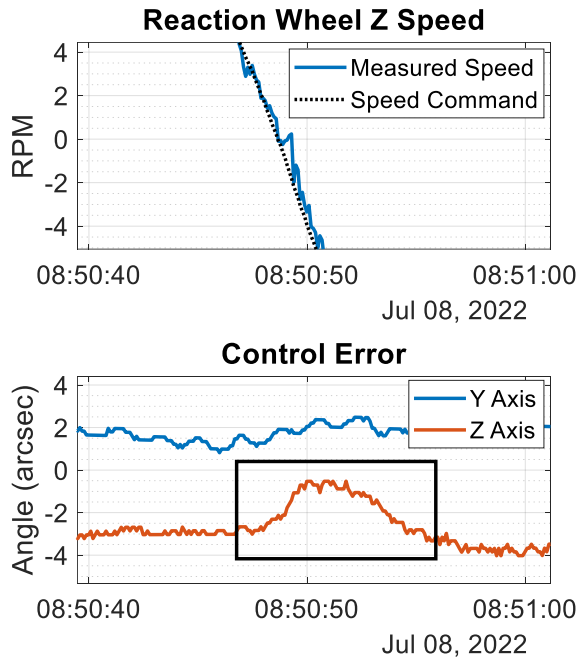

Figure 9: Control Error Transient Induced by NRW Zero Crossing

telemetry from similar TOC flown CubeSats, were implemented in simulation to study the effect on pointing performance. Simulation results indicated pointing error transients occur at zero-crossings, but the magnitude was not appreciable enough to cause a loss of link during closed-loop operations. Figure 9 shows PTD-3 flight telemetry where a zero crossing occurs while controlling with payload in the loop. There is a noticeable control error transient in the Z axis in response to the zero crossing from the Z reaction wheel. The frequency of these crossings is low and has not disrupted payload operations.

End-to-End Pointing Simulations

The TOC high-fidelity 6-DOF spacecraft simulation was used during the design phase to verify new software functions and predict performance. The simulation includes high-fidelity sensor and actuator models including the reaction wheel stiction to capture the dynamic effects of zero-crossings. A payload model with representative sensor noise characteristics provided by MIT Lincoln Laboratory was integrated into the simulation to accurately predict payload-in-the-loop pointing performance. The simulation also includes the GNC algorithms which are auto coded into the flight software.

A comprehensive set of Monte Carlo test cases were simulated to understand sensitivities and predict performance metrics in presence of random uncertainties and reaction wheel zero crossings. Test cases varied critical spacecraft sources of error including actuator/sensor alignments, vehicle mass properties, sensor noise properties, and orbit pass geometries. The

Table 4: PTD-3 Pointing Budget

Line Item	Error Sources	Value	Units
Initial Acquisition Phase			
1	Bus Attitude Knowledge	26.8	arcsec
2	Payload-to-Bus Misalignment (Post On-Orbit Calibration)	50	
3	**Attitude Knowledge (1+2)**	76.8	
4	Control	37.5	
5	RW Jitter	1	
6	**Pointing Accuracy (3+4+5)**	115.3	
	Requirement	900	
	Margin	**681%**	
Payload-in-the-Loop Pointing			
1	Control	3.5	arcsec
2	RW Jitter	1	
3	**Pointing Accuracy (1+2)**	4.5	
	Requirement	6.2	
	Margin	**38%**	

results of the Monte Carlo simulation cases informed various line items in the pointing budget shown in in Table 4. During the initial acquisition phase, the budget shows significant margin against the requirement, providing confidence the vehicle can acquire signal lock with the ground station. For payload-in-the-loop pointing, no allocation for misalignment and bus attitude knowledge are included since the bus pointing control loop is closed around direct payload measurements. The pointing accuracy was predicted to be 4.5 arcseconds, which is within the bus pointing requirement and supports the bus capability to maintain link with the ground optical terminal.

Orbit Propagation Accuracy using Two Line Elements (TLEs)

During the initial acquisition phase of payload tracking, the optical ground terminal uses knowledge of the spacecraft ephemeris to acquire and track PTD-3. The

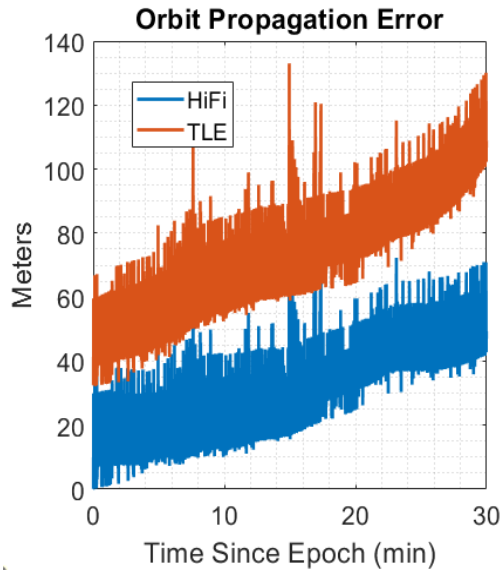

Figure 10: Comparing orbit propagation accuracy using TLEs versus HiFi orbit propagation models

ground station architecture is limited to using Two Line Elements (TLEs), which rely on lower accuracy SGP4 orbit propagation models, to predict satellite ephemeris during a lasercomm pass. Spacecraft TLEs can be readily obtained through the externally published NORAD catalog, however these TLEs were insufficient to predict spacecraft position to the 100m accuracy required for the optical ground terminal to acquire PTD-3 for lasercomm payload demonstrations. To meet the requirement, a custom TLE was generated from PTD-3s onboard position, velocity, and time (PVT) telemetry derived from GPS. For this mission, the process for converting the onboard PVT telemetry into a TLE was automated as follows. Approximately 30 minutes prior to a payload pass, the spacecraft downlinks onboard PVT telemetry to the ground. Next, the ground runs a script that takes the PVT telemetry from the database and runs the TLE generation tool. The refined TLE output from the tool is automatically emailed to the ground operators and engineers responsible for executing payload experiments using the optical ground terminal.

Figure 10 compares the error associated with ephemeris predictions using a TLE versus a high-fidelity (HiFi) orbit propagator. For both propagators, the error represents the difference between the predicted spacecraft position from the orbit propagation model and PVT flight telemetry derived from PTD-3's onboard GPS. In this example, the TLE method remains below the 100m position requirement for the majority of the 30-minute propagation. The ability to use a HiFi orbit propagator would have resulted in better spacecraft tracking performance and would enable longer than 30-minute propagation times. Nonetheless, the automated TLE generation solution proved sufficiently accurate for the optical ground terminal to acquire PTD-3 during payload demonstration passes.

ON-ORBIT OPERATIONS

PTD-3 has successfully completed many payload-in-the loop passes, the most recent of which achieved pointing accuracy performance less than 1 arcsec at vehicle body rates as high as 0.9°/s. To the author's knowledge, this is the most accurate body steered pointing accuracy achieved by a CubeSat to date.

The first successful demonstration with payload-in-the-loop pointing occurred approximately 1-month after launch in June 2022. Figure 11 shows the timeline of events for a typical payload demonstration. The timeline begins with the spacecraft slewing to track a radio frequency (RF) station for telemetry, tracking, and command purposes. This occurs approximately 30-

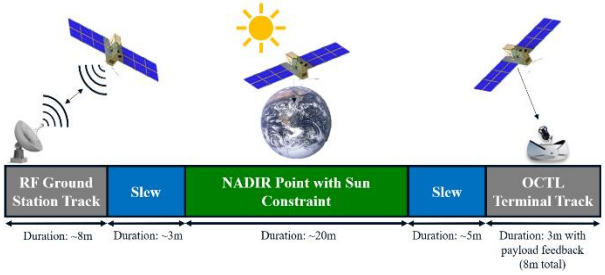

Figure 11: Mission Timeline Overview. The vehicle is tasked with several slews prior to the ground track of the OCTL terminal.

minutes before the pass over OCTL. During the RF pass, the spacecraft's PVT telemetry, derived from onboard GPS, is downlinked to a ground server to create a TLE with the most recent spacecraft ephemeris and is

described in earlier sections. An automated process ingests the spacecraft PVT telemetry, generates an updated TLE, and delivers it electronically to the OCTL within several minutes of establishing communications with the RF ground station. After the RF pass completes, PTD-3 slews back to a NADIR pointing attitude where it remains until beginning the autonomous transition to track the OCTL. The spacecraft initiates a slew 5-minutes prior to the OCTL being in-view to allow for

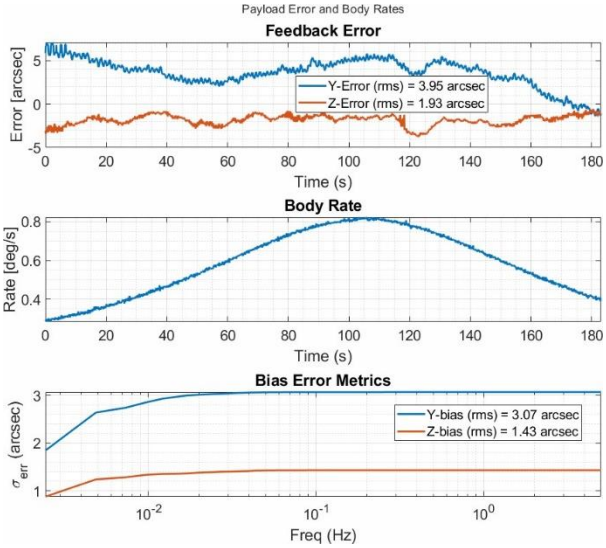

Figure 12: Performance Metrics for the July 21st, 2022 pass, prior to controller updates.

sufficient time to settle prior to tracking. Nominally, slewing and settling occurs in less than 3 minutes. After beginning the track of the OCTL, the onboard software autonomously transitions to payload-in-the-loop pointing when valid control error feedback from the payload is available with sufficient persistency.

Early On-Orbit Performance

Pointing performance results from a pass on July 21st, 2022 can be seen in Figure 12. The RMS pointing errors for the Y and Z axes over the duration of the pass were 3.95 arcsec and 1.93 arcsec, respectively. The bias for the Y and Z axes were 3.07 and 1.43 arcsec, respectively. The spacecraft body rate peaked at 0.8°/s with wheel speeds remaining below 2000 RPM. The bus pointing performance capabilities successfully met the mission pointing requirements for acquiring, establishing, and maintaining the space to ground lasercomm link. Given pointing performance was sufficient to meet mission needs for the on-going payload demonstration passes, no immediate efforts were pursued to improve performance. However, the presence of a low-frequency bias was persistently evident in the payload feedback error as shown in results presented in Figure 12, and in the several dozen subsequent passes that occurred over the following year.

This bias is due to moment of inertia (MOI) uncertainty in the system and environmental disturbances, primarily caused by aerodynamic drag.

The MOI value is estimated from mechanical CAD models, which are predicted to have errors on the order 5-15%. The estimate is used in the vehicle's feedforward loop (comprised of acceleration and gyroscopic components) to generate torques for target tracking. Any offsets between the flight estimate and the vehicle's true MOI enter the control loop as an effective steady-state disturbance on the vehicle which can contribute to the

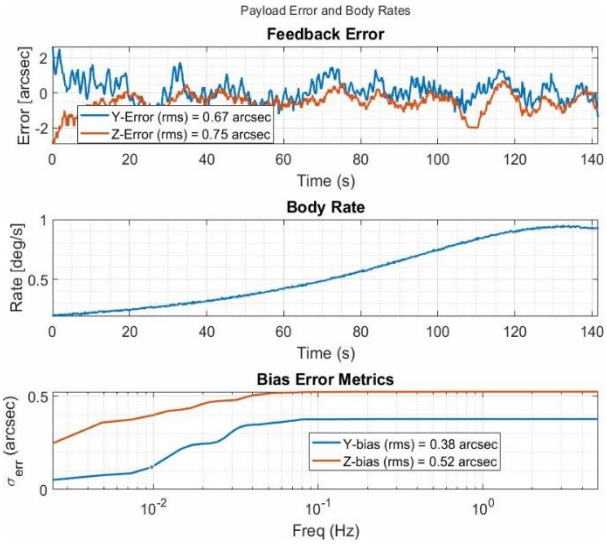

Figure 13: Performance Metrics for the May 30th, 2023 pass, after controller updates

pointing biases observed on-orbit. The feedforward torque component drives most of the pointing dynamics over the duration of the lasercomm pass with a relatively minor contribution from the payload feedback error.

Aerodynamic drag torque is the largest environmental disturbance present in PTD3's orbit regime. It is a function of center of pressure to center of mass offset and the atmospheric density. This is another component influencing the observed pointing bias.

Post-Tuning On Orbit Performance

The opportunity to implement a controller update to address the low-frequency bias present in the feedback error was implemented nearly a year after launch in May 2023. The updates included an increase to the overall controller bandwidth and increase in integrator gain to compensate for the steady state error. The controller updates were implemented on the spacecraft prior to the

May 30th, 2023 pass whose results are shown in Figure 13.

The RMS pointing error for Y and Z axes over the pass were 0.67 and 0.75 arcsec, respectively. The bias for the Y and Z axes were improved by an order of magnitude to 0.38 and 0.52 arcsec, respectively. The peak body rate observed over the portion of this pass was 0.9°/s. Note that telemetry from the latter half of the pass is missing from Figure 13 due to a dropout unrelated to pointing accuracy. To the author's knowledge, the sub-arcsecond pointing accuracy demonstrated on PTD-3 represents the best body steered CubeSat pointing performance achieved during a high-rate ground track.

Extended On Orbit Operations

Due to the ongoing success of PTD-3, mission operations were extended beyond the planned 4-month period. PTD-3 operations have been ongoing for over 2-years now. Vehicle deorbit is currently the time limiting factor for continuing to support mission operations. Since propulsion is not incorporated in the design to compensate for atmospheric drag, TOC has resorted to other creative concepts for extending the mission life. This has been particularly challenging due the near solar max conditions of the current sun cycle, which has led to higher air densities and quicker orbital decay. In early 2023, flight telemetry combined with orbit simulation predictions indicated a complete deorbit by early January 2024. To extend the lifetime, multiple strategies were employed.

In March 2023, the nominal attitude of the vehicle was updated to a low drag attitude configuration, that minimizes the projected area of the vehicle in the velocity direction, while still maintaining enough solar power to execute all nominal and payload operations. Additionally, the number of telemetry downlink passes were reduced by 60% to minimize slewing and drag inefficient attitudes. Currently, the vehicle is taking approximately 1 pass per orbit to downlink nominal state of health telemetry with additional passes added to support payload operations. After implementation of the low drag attitude and reduced downlink passes, the average projected area in the velocity direction was reduced from 0.4m^2 to 0.09m^2.

The current deorbit analysis shown in Figure 14 predicts PTD-3 will deorbit in October 2024, which represents an increase of an additional 10 months from the original deorbit date enabled by the updated low drag attitude configuration. The current operations and bus performance is expected to be nominal until the altitude falls below 350 km. There is potential for operations to continue at lower than 350 km, but requires further analysis with potential updates to software and/or CONOPs.

An additional objective for the extended mission period is to demonstrate payload pointing at different optical ground stations. The spacecraft is currently executing extended payload operations with the Low-Cost Optical Terminal (LCOT) at NASA's Goddard Space Flight Center in Greenbelt, and the Optical Ground Station 2 (OGS-2) in Haleakala, Hawaii.[9]

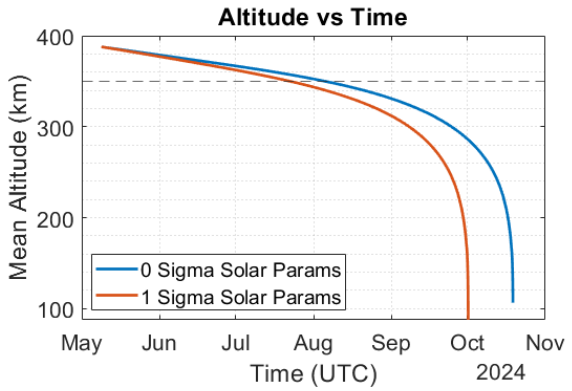

Figure 14: Predicted Deorbit Timeline

CONCLUSION

The sub-arcsecond pointing accuracy PTD-3 demonstrated on orbit highlights the impressive capabilities offered by CubeSat platforms. PTD-3's implementation of a bus attitude control architecture that leverages low noise line-of-sight error measurements directly from the payload combined with high performance TOC reaction wheels and avionics enabled RMS pointing accuracy of 0.75 arcsecond (worst axis). This performance was achieved during body rates as high as 0.9°/s, and is currently the best demonstrated performance for similarly sized spacecraft utilizing body steering.

The PTD-3 CubeSat remains in a low drag attitude configuration to extend on orbit mission life in support of payload operations with different ground optical terminals. As the orbit lowers, there will be additional opportunities to demonstrate sub-arcsecond pointing accuracy at even higher tracking rates in the presence of larger aerodynamic disturbances.

ACKNOWLEDGEMENTS

The authors would like to acknowledge the dedication and efforts of Allan Shtofenmakher for technical stewardship throughout the program, Liam Bruno for early program GNC design and development contribution, and Jacob Beaver for mission operations support. The authors also acknowledge the support of Dave J. Mayer from NASA Ames Space Research

Center throughout the design and build of PTD-3 and Beth A. Keer from NASA Goddard Space Flight Center during on-orbit operations. The authors would also like to thank MIT LL for payload development, integration support, and on-going operations support.

REFERENCES

1. Riesing, Kathleen M., Curt M. Schieler, Jesse S. Chang, Noah J. Gilbert, Andrew J. Horvath, Robert S. Reeve, Bryan S. Robinson, Jade P. Wang, Paaras S. Agrawal, and Robert A. Goodloe. "On-orbit results of pointing, acquisition, and tracking for the TBIRD CubeSat mission." In Free-Space Laser Communications XXXV, vol. 12413, pp. 25-33. SPIE, 2023.

2. Pong, C. M., "On-Orbit Performance & Operation of the Attitude & Pointing Control Subsystems on ASTERIA", Proceedings of the 32rd Annual AIAA/USU Conference on Small Satellites, Logan, UT, August 2018, SSC18-PI-34.

3. Mason, James Paul, Thomas N. Woods, Phillip C. Chamberlin, Andrew Jones, Rick Kohnert, Bennet Schwab, Robert Sewell et al. "MinXSS-2 CubeSat mission overview: Improvements from the successful MinXSS-1 mission." Advances in Space Research 66, no. 1 (2020): 3-9.

4. Rose, Todd S., Darren W. Rowen, S. LaLumondiere, Nicolette I. Werner, Roberto Linares, A. Faler, J. Wicker et al. "Optical communications downlink from a 1.5 U CubeSat: OCSD program." In International Conference on Space Optics—ICSO 2018, vol. 11180, pp. 201-212. SPIE, 2019.

5. Menegaldo, Cauê G., Fábio de O. Fialho, Eduardo Janot-Pacheco, Felipe M. Pait, and Vincent Lapeyrère. "PicSat's enduring legacy. Probing the flight of a small astronomical satellite." Publications of the Astronomical Society of the Pacific 134, no. 1033 (2022): 034501.

6. Simonetti, Simone, Valerio Di Tana, Gabriele Mascetti, Simone Pirrotta, and Edmondo Scorzafava. "ArgoMoon: Italian CubeSat Technology to Record the Maiden Flight of SLS Towards the Moon." (2020).

7. Ikari, Satoshi, Masahiro Fujiwara, Hirotaka Kondo, Shuhei Matsushita, Ichiro Yoshikawa, Kazuo Yoshioka, Reina Hikida et al. "Solar system exploration sciences by equuleus on sls em-1 and science instruments development status." (2019).

8. J. Vanderlei Martins, Tim Nielsen, Chad Fish, Leroy Sparr, Roberto Fernandez-Borda, Mark Schoeberl, Lorraine Remer. "HARP CubeSat–An innovative HyperangularImaging Polarimeter for Earth Science Applications." Small Sat Pre-Conference Workshop, Logan, Utah. (2014).

9. Schauer, Katherine, "New Ground Station Brings Laser Communications Closer to Reality," NASA, August 2020, www.nasa.gov/missions/tech-demonstration/new-ground-station-brings-laser-communications-closer-to-reality/